CFD Investigations of Subcooled Nucleate Boiling Flows and Acting Interfacial Forces in Concentric Pipes

Achref Rabhi[1] Ioanna Aslanidou[1] Konstantinos Kyprianidis[1] Rebei Bel Fdhila[1,2]

[1]Future Energy Center, Mälardalen University, Sweden,
{achref.rabhi,ioanna.aslanido,konstantinos.kyprianidis,rebei.bel.fdhila}@mdh.se
[2]Hitachi ABB Power Grids, Sweden, rebei.bel_fdhila@hitachi-powergrids.com

Abstract

Boiling flows are widely encountered in several engineering and industrial processes. They have a special interest in nuclear industry, where a Computational Fluid Dynamic (CFD) thermohydraulic investigation becomes very popular for design and safety. Many attempts to model numerically subcooled nucleate boiling flows can be found in the literature, where several interfacial forces acting on bubbles which are interacting on the bulk fluid were neglected, due to the hard convergence of the calculations, or to the bad accuracy of the obtained results. In this paper, a sensitivity analysis is carried out for the interfacial forces acting on bubbles during subcooled nucleate boiling flows. For this purpose, 2D CFD axisymmetric simulations based on an Eulerian approach are performed. The developed models aim to mimic the subcooled nucleate boiling flows in concentric pipes, operating at high pressure. The predicted spatial fields of boiling quantities of interest are presented and commented. The numerical results are compared against the available experimental data, where it is shown that neglecting some interfacial forces like the lift or the wall lubrication forces will yield to good predictions for some quantities but will fail the prediction for others. The models leading to the best predictions are highlighted and proposed as recommendations for future CFD simulations of subcooled nucleate boiling flows.

Keywords: subcooled nucleate boiling flows, computational fluid dynamics, interfacial forces, sensitivity analysis

1 Introduction

Subcooled nucleate boiling flows are present in several engineering equipment and devices, such as nuclear reactors, heat exchangers and cooling systems. They are associated with hydrodynamics, heat and mass transfer. These flows have gained a special interest because of their enhanced heat transfer coefficients and improved heat transfer performance. Subcooled nucleate boiling flows are two-phase, composed by a continuous subcooled liquid phase, and a vapor dispersed phase, generated by separate bubbles. These bubbles are nucleated from micro-cavities, referred to as nucleation sites, randomly distributed over a heated surface, when the latter's temperature exceeds the working liquid saturation temperature at the local pressure. Bubbles depart their nucleation sites when reaching a critical size, referred as bubble departure diameter. They slide along the heated surface, and lift-off to the core of the liquid, where they migrate into the subcooled region of the flow. In this region, bubbles are subject to condensation when the local flow temperature is lower than the saturation temperature. Hence, the two-phase boiling flow is referred as subcooled boiling flow.

In order to improve thermal management system design and to maximize heat transfer coefficients, high-fidelity models need to be incorporated. Experiments can be used successfully to fulfill this task. However, they are still very expansive and time consuming to perform. Eulerian two-fluid models based on CFD simulations are a promising solution to develop such high-fidelity representations, where the flow structure, transport phenomenon and interactions between phases can be well predicted. The vapor-averaged void fraction, width of two-phase layer near the heated surface and temperature fields, which are crucial for design and optimization, can be very well and accurately presented. Turbulence effects can also be incorporated through these models. One of the most successful Eulerian two-fluid model for boiling flows was developed by Kurul and Podowski (1990), where they decomposed the total applied heat flux at the wall on three components; the first accounts for the evaporation, the second accounts for the quenching contribution and the last is responsible for heating the liquid near the heated surface when bubbles are absent.

Based on the same framework approach, and applying some slight modifications, many authors simulated the subcooled nucleate boiling flows in different geometries at multiple operating conditions, and compared their numerical results to their experimental data, or data from literature (Lai and Farouk, 1993; Anglart and Nylund, 1996; Roy et al., 2001; Končar et al., 2004). However, no sensitivity analysis quantifying the effect of the used interfacial forces models was carried out, despite that the dispersed-phase spatial distribution is highly affected by these forces, in addition to the turbulent behavior of the flow, that will in turn significantly influence the hydrodynamics and the thermal process, including heat and mass transfer (Končar et al., 2004). Hence, the obtained results

were acceptable for some fields, but failed for many others. Also, the bubble's size in the bulk fluid was ignored, despite its importance for such flows and its major effect on heat transfer, temperature fields, void fraction distribution and the two-phase layer thickness.

A first model to predict the bubble size evolution in the bulk fluid was proposed by Ishii et al. (2005) via the Interfacial Area Transport Equation (IATE), where the authors proposed empirical model coefficients to take into account the coalescence and the turbulent break-up phenomenons. The IATE model and the proposed coefficients by Ishii et al. (2005) were adopted in CFD simulations by Končar and Krepper (2008) and Michta (2011) among others, for high pressure boiling in conventional sized channels, and by Rabhi and Bel Fdhila (2019) for low pressure boiling in narrow channels. However, the bubbles bulk diameter was not very well predicted, and affected the accuracy of the computed fields. This is due to the used model coefficients which are not applicable for different geometries and operating conditions. In addition, the IATE model depends on the used interfacial forces, but, as highlighted previously, a sensitivity analysis and a quantification of these forces are missing, and represents a research gap for boiling flows modeling. However, assuming a constant bubble bulk diameter model, set to the mean value of the experimentally measured bubble bulk diameter, represents a good approximation, and yields to acceptable predictions as it will be shown in this work.

In the present work, 2D axisymmetric CFD simulations based on an Eulerian two-fluid approach are carried out modeling the subcooled nucleate boiling flow of refrigerant R-113 flowing upward a concentric pipe at an absolute pressure of 2.69 bar. The CFD model is implemented on the open-source CFD platform OpenFOAM, where a Finite-Volume discretization of the governing transport equations is adopted. The spatial distributions of boiling quantities predicted by the CFD calculations are presented and analyzed. The effect of the interfacial forces on the predicted fields are investigated. The model predictions are compared against the available experimental data of Roy et al. (2001), and these models yielding to successful predictions are highlighted and proposed as recommendations for future subcooled nucleate boiling flows CFD simulations.

2 Mathematical model

Based on the Eulerian two-fluid framework, transport equations, i.e., mass, momentum, energy and turbulence, are solved for the continuous liquid phase and the dispersed vapor phase.

2.1 Transport equations

Neglecting the small density variation with temperature rise, for each phase k, the mass conservation transport equation is written as:

$$\frac{\partial \alpha_k \rho_k}{\partial t} + \nabla.(\alpha_k \rho_k \mathbf{U}_k) = \Gamma_{ki} - \Gamma_{ik} \tag{1}$$

where α is the void fraction, ρ is the fluid density, $\mathbf{U}$ is the velocity vector and Γ is mass transfer rate, that denotes mass transfer rate per unit volume due to evaporation from the liquid phase to the vapor phase or mass transfer rate per unit volume by condensation from the vapor phase to the liquid phase, that their expression will be given in the boiling model section.

The momentum transport equation for each phase is given by:

$$\begin{aligned}\frac{\partial \alpha_k \rho_k \mathbf{U}_k}{\partial t} + \nabla.(\alpha_k \rho_k \mathbf{U}_k \mathbf{U}_k) = -\alpha_k \nabla p + \mathbf{R}_k \\ + \mathbf{M}_k + \alpha_k \rho_k \mathbf{g} + (\Gamma_{ki}\mathbf{U}_i - \Gamma_{ki}\mathbf{U}_k)\end{aligned} \tag{2}$$

where the first term in the right hand side corresponds to the pressure drop contribution, the second term $\mathbf{R}_k$ denotes the combined turbulent and viscous stress, the third term $\mathbf{M}_k$ represents the interfacial momentum transfer contribution, that will be detailed in the next section, the fourth term represents the gravity contribution and the last term accounts the contribution of mass transfer between phases to the momentum.

In this work, energy transport equation for each phase k is solved in terms of the specific enthalpy h. It is written for each phase as:

$$\begin{aligned}\frac{\partial \alpha_k \rho_k h_k}{\partial t} + \nabla.(\alpha_k \rho_k \mathbf{U}_k h_k) = \alpha_k \frac{Dp}{Dt} \\ + \nabla\left(\alpha_k D_{t,k}^{eff} \nabla h_k\right) + \Gamma_{ki} h_i - \Gamma_{ik} h_k + Q_{wall,k}\end{aligned} \tag{3}$$

where Dp/Dt is the material derivative of the pressure, $Q_{wall,k}$ is the product of the applied heat flux on the wall q_w'' and the contact area with the wall per unit volume, and $D_{t,k}^{eff}$ is the effective thermal diffusivity, that includes the turbulent contribution, given by:

$$D_{t,k}^{eff} = \frac{\lambda_k}{C_{p,k}} + \frac{\mu_k^t}{\mathrm{Pr}^t} \tag{4}$$

where λ_k is the thermal conductivity, $C_{p,k}$ is the specific heat capacity, μ_k^t is the dynamic turbulent viscosity and Pr^t is the turbulent Prandtl number, set to a constant equal to 0.85.

To account the turbulent behavior of both phases, continuous and dispersed, the standard $k-\varepsilon$ turbulence model is used. For each phase, the turbulent kinetic energy k and its dissipation ε are calculated. The $k-\varepsilon$ turbulence model is adopted here because of its valid for fully turbulent flows, which is the case of the simulated problem here with a Reynolds number of 34450. It stills computationally cheap and robust turbulence model for pipes flows where there are no flow recirculation, despite its known limitations, rising principally from its empirical coefficients. However, this model lacks of sensitivity to adverse pressure gradients, and performs poorly for complex flows. In this work, the bubble induced turbulence was accounted by a turbulent kinematic viscosity as:

$$\nu_l^{t,b} = \frac{C_{\mu,b} d_b \alpha_v}{2} ||\mathbf{U}_v - \mathbf{U}_l|| \tag{5}$$

where $C_{mu,b}$ is a coefficient set to 1.2 following the recommendations of Sato et al. (1981) for bubbly flow modeling, and d_b is the bubble bulk diameter, calculated via a constant bubble bulk diameter model. This bubble bulk diameter is set to the mean value of the experimental measured diameters by Roy et al. (2001).

2.2 Interfacial forces

For boiling flows, the relevant interfacial forces that should be included in the momentum equation are the drag, added mass, lift, wall lubrication and turbulent dispersion forces. In the following, the physical interpretation, mathematical and force coefficient models are presented.

Drag force

The drag force $\mathbf{F}_D$ models the resistance experienced by a bubble opposed to its motion, created by the surrounding fluid. Its mathematical expression is given by:

$$\mathbf{F}_D = -\frac{3}{4} C_D \frac{\alpha_v \rho_l}{d_b} \|\mathbf{U}_v - \mathbf{U}_l\| (\mathbf{U}_v - \mathbf{U}_l) \tag{6}$$

where C_D is the drag force coefficient. In this work, two different coefficient models are tested. The first model is the classic solid sphere drag model, proposed by Schiller and Naumann (1935) as:

$$C_D = \begin{cases} 24\left(1 + 0.15\mathrm{Re}_b^{0.687}\right) & \text{if } \mathrm{Re}_b \leq 1000 \\ 0 & \text{else.} \end{cases} \tag{7}$$

where Re_b is the bubble Reynolds number. The second is the model of Tomiyama et al. (1998), which was developed for bubbly flow. This model is written as:

$$C_D = \max\left(\frac{16}{\mathrm{Re}_b}\min\left(1 + 0.15\mathrm{Re}_b^{0.687}, 3\right), \frac{8}{3}\frac{\mathrm{Eo}}{\mathrm{Eo}+4}\right) \tag{8}$$

where Eo is the Eötvös number.

Added mass force

The acceleration of bubbles in the flow accelerates the surrounding fluid itself, which adds an apparent mass to the bubbles. This is modeled by the virtual mass force $\mathbf{F}_{VM}$, which is given by:

$$\mathbf{F}_{VM} = -C_{VM} \frac{1 + 2\alpha_v}{\alpha_l} \alpha_v \left(\frac{D\mathbf{U}_v}{Dt} - \frac{D\mathbf{U}_l}{Dt}\right) \tag{9}$$

where C_{VM} is the virtual mass coefficient set to a constant equal to 0.5 in this work following the recommendations of Zuber (1964) for spherical bubbles.

Lift force

The lift force $\mathbf{F}_L$ is caused by the velocity gradient across the dispersed phase. It is responsible for a pressure difference across the walls and creates a force towards the side. Its general mathematical expression is written as:

$$\mathbf{F}_L = C_L \alpha_v \alpha_l (\mathbf{U}_v - \mathbf{U}_l) \times \nabla \times \mathbf{U}_l \tag{10}$$

where C_L is the lift force coefficient. In this work, a constant lift force coefficient models are used, set to 0.05 and 0.5, in addition to the model of Tomiyama et al. (2002), proposed as following:

$$C_D = \begin{cases} \min\left(0.288\tanh\left(0.12\mathrm{Re}_b\right), f(\mathrm{Eo})\right) & \text{if } \mathrm{Eo} \leq 4 \\ f(\mathrm{Eo}) & \text{if } 4 \leq \mathrm{Eo} \leq 10.7 \\ -0.288 & \text{else.} \end{cases} \tag{11}$$

with:

$$f(\mathrm{Eo}) = 1.0422\ 10^{-3}\mathrm{Eo}^3 - 1.59\ 10^{-2}\mathrm{Eo}^2 - 2.04\ 10^{-2}\mathrm{Eo} + 0.474 \tag{12}$$

Wall lubrication force

In the two-fluid Eulerian modeling approach, the near wall effects are captured by the wall lubrication forces $\mathbf{F}_{WL}$. These forces are accounted for repulsive effects pushing the bubbles away from the wall, referred usually as wall peaking effects. The mathematical expression of $\mathbf{F}_{WL}$ is given by:

$$\mathrm{F}_{WL} = -C_{WL}\alpha_v\rho_v\|\mathbf{U}_r - (\mathbf{U}_r.\mathbf{n}_w)\,\mathbf{n}_w\|^2\mathbf{n}_w \tag{13}$$

where $\mathbf{U}_r$ is the relative velocity, $\mathbf{n}_w$ is the unity vector normal to the wall and C_{WL} is the force model coefficient, calculated based on the models of Antal et al. (1991) and Franc (2005). The Antal et al. model is given by:

$$C_{WL} = \max\left(0, \frac{C_{w,1}}{d_b} + \frac{C_{w,2}}{y_w}\right) \tag{14}$$

where the parameters C_{w1} and C_{w2} are set to -0.01 and 0.05 respectively (Frank, 2005), d_b is the bubble diameter and y_w is the bubble center distance to the nearest wall. The Frank model is written as:

$$C_{WL} = C_{w,3}(\mathrm{Eo}) \max\left(0, \frac{1 - \frac{y_w}{C_{w,c}d_b}}{y_w C_{w,d}\left(\frac{y_w}{C_{w,c}d_b}\right)^{p-1}}\right) \tag{15}$$

where $C_{w,3}(\mathrm{Eo})$ is given as following:

$$C_{w,3} = \begin{cases} \exp\left(-0.933\mathrm{Eo} + 0.179\right) & \text{if } \mathrm{Eo} \leq 5 \\ 5.99\ 10^{-3}\mathrm{Eo} - 0.0187 & \text{if } 6 < \mathrm{Eo} \leq 33 \\ 0.0179 & \text{else.} \end{cases} \tag{16}$$

with $C_{w,c}$, $C_{w,d}$ and p are a cut-off coefficient, a damping coefficient and a power, set to 10, 6.8 and 1.7, respectively (Frank, 2005).

Turbulent dispersion force

The turbulent dispersion force $\mathbf{F}_{TD}$ originates from the dispersions of bubbles, caused by fluctuations and eddies of the turbulent flow. The Lopez de Bertodano (1991) and the Burns et al. (2004) models are compared in this work. The Lopez de Bertodano model is mathematically expressed as:

$$\mathbf{F}_{TD} = C_{TD}\rho_l k_l \nabla\alpha_v \tag{17}$$

while the Burns et al. model is given by:

$$\mathbf{F}_{TD} = \frac{3}{4} C_{TD} \mathrm{Re}_b \frac{\nu_v \nu_v^t}{\sigma d_b^2} \rho_v \left(1 + \frac{\alpha_l}{\alpha_v}\right) \tag{18}$$

where C_{TD} is the turbulent dispersion force coefficient, set to 0.4 and 1.0 for comparison, and ν_v and ν_v^t are the vapor phase kinematic and turbulent kinematic viscosities.

2.3 Boiling model

The boiling model adopted in this work follows the version of the very well known RPI (Rensselaer Polytechnic Institute) model proposed by Kurul and Podowski (1990). This model proposes to decompose the total applied heat flux $q_w^{"}$ at the wall into three components; convective heat flux $q_{w,c}^{"}$ that is responsible for heating the liquid near the surface when there are no bubbles in contact with it, evaporative heat flux $q_{w,e}^{"}$ that is accounted for the liquid evaporation to create bubbles, and quenching heat flux $q_{w,q}^{"}$ that represents the transient conduction while the liquid is filling the previous occupied volumes by departing bubbles. This decomposition is written as:

$$q_w^{"} = q_{w,c}^{"} + q_{w,e}^{"} + q_{w,q}^{"} \tag{19}$$

The mathematical expressions of each heat flux contribution can be found in (Kurul and Podowski, 1990). The RPI model needs to be fed with closure equations that are applied at the heated surface, as the active nucleation site density N_a, the bubble departure diameter d_{dep} and the bubble departure frequency f_{dep}. These latter boiling closures are considerably affected by the heated surface roughness. It can increase the number of the nucleation sites, and controls the bubble shape and release rate. However, despite its major effect on bubble formation rates, the wall roughness will not be considered in this work, and the basic boiling closure equations neglectingthis parameter are adopted here. The reformulated model of Lemmert and Chawla (1977) by Egorov and Menter (2004) is used to model here the active nucleation site density. It is given by:

$$N_a = N_{a,ref} \left(\frac{\Delta T_{sup}}{\Delta T_{ref}}\right)^{1.805} \tag{20}$$

where the empirical coefficient $N_{a,ref}$ is set to 9.922 10^5 sites/m^2 following the recommendations of Egorov and Menter (2004), ΔT_{sup} is the wall superheat that is equal to the difference between the wall temperature and the liquid saturation temperature, and ΔT_{ref} is a reference temperature difference, set to 10 K. For the bubble departure diameter calculations, a modified version of the model of Tolubinski and Kostanchuk (1970) which is given as following is adopted:

$$d_{dep} = d_{ref} \exp\left(\frac{\Delta T_{sub,y^+=250}}{\Delta T_{ref}}\right) \tag{21}$$

where d_{ref} and ΔT_{ref} are reference bubble departure diameter and temperature difference, set to 0.6 10^{-3} m and 45 K, respectively, following the recommendations of Tolubinski and Kostanchuk (1970), and $\Delta T_{sub,y^+=250}$ is a modified subcooling temperature, calculated based on the liquid temperature at a distance from the wall based on the wall function at $y^+ = 250$. The last closure equation for the boiling model is the bubble departure frequency model, calculated based on the Cole (1960) model as:

$$f_{dep} = \sqrt{\frac{4g(\rho_l - \rho_v)}{3 d_{dep} \rho_l}} \tag{22}$$

The last quantities calculated by the boiling model are the evaporation and the condensation rates Γ_{lv} and Γ_{vl}, that are needed to solve the transport equations. They are given by:

$$\Gamma_{l,v} = \frac{A_{w,b,e}^f}{6} \rho_v d_{dep} f_{dep} \tag{23}$$

$$\Gamma_{v,l} = \frac{h_c (T_{sat}(p) - T_l)}{h_{lg}} A_s \tag{24}$$

where $A_{w,b,e}^f$ is an area fraction of the heated surface not affected by bubbles and h_c is a condensation heat transfer coefficient calculated based on the correlation of Ranz and Marshall (1952).

3 Computational Domain and Solution Procedure

The computational domain is illustrated through Figure 1. It consists of 2D axisymmetric concentric pipe, having inner and outer diameters r_{in} and r_{out} equal to 7.89 mm and 19.01 mm, respectively. The concentric pipe is heated only from the inner upper side, by applying a constant uniform heat flux, allowing an adiabatic section for the flow development. Refrigerant R-113 flows downstream the adiabatic section of 0.91 m and then in 2.75 m heated section. The total flow length is 3.66 m. The computational domain is meshed using 20496 hexahedron elements, corresponding to 56 elements in the radial direction needed

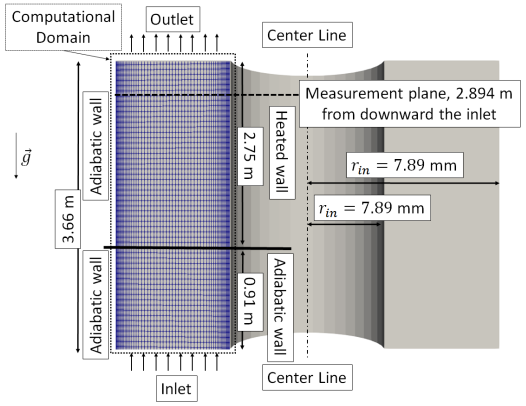

Figure 1. Computational domain and mesh.

for the grid convergence and 366 element in the flow direction. Near each wall, 20% of the radial length is meshed with refined elements to represent the viscous layers. The refined elements represent 30% of the radial elements with a expansion ratio of 0.25 at each wall normal direction.

At the pipe inlet, the pressure is set to 2.69 bar, corresponding to a saturation temperature of 80.5°C for R-113. Constant velocity and temperature are applied, set to 0.522 m/s and 50.2°C, respectively. This corresponds to an inlet Reynolds number and subcooling equal to 34450 and 30.3°C. A non-slip boundary condition is used for both phases velocities at the channel walls, and a constant uniform heat flux is applied only at the inner heated wall of length 2.75 m, set to 116000 W/m^2. Only in this part of the wall, the boiling closure equations are applied. At the channel outlet, a pressure gradient boundary condition is applied. The refrigerant R-113 thermophysical properties are calculated at the inlet based on the corresponding temperature and pressure. However, the developed CFD model allows the calculation of the local saturation temperature based on the corresponding predicted local pressure. For this purpose, an interpolation is performed on R-113 saturation tables.

The open-source CFD platform OpenFOAM is used to solve the transport equations with respect to the previous described computational domain and operating conditions. A Finite-Volume discretization technique is employed, where the spatial derivatives including the void fraction are discretized based on Van Leer scheme, the gradient and divergence terms are based on a Gauss upwind schemes, while the Laplacians are based on Gauss linear schemes. A semi-explicit temporal discretization is adopted for the temporal derivatives, in order to accelerate the convergence of the simulations. The discretized equations are solved based on the Geometric-Algebraic Multi-Grid (GAMG) solver for the pressure, and iterative symmetric Gauss-Seidel smooth solver is used for the rest of the variables. The PIMPLE algorithm is employed to solve the pressure-velocity coupling.

4 Results and discussions

The void fraction, liquid temperature, liquid and vapor magnitude velocity fields predicted by the CFD calculations are presented in Figure 2. Despite that the simulations were carried out in a 2D axisymmetric geometry, having a total flow length of 3.66 m, the fields were extruded rotationally and re-scaled for a better comprehensible representation. These results are obtained with calculations using Schiller and Naumann (1935) drag model, a constant virtual mass coefficient model equal to 0.5, Antal et al. (1991) wall lubrication model and Burns et al. (2004) turbulent dispersion model. These interfacial forces are adopted for the fields representation since they give the best predictions with comparison to the experimental data of Roy et al. (2001) as it will be shown later.

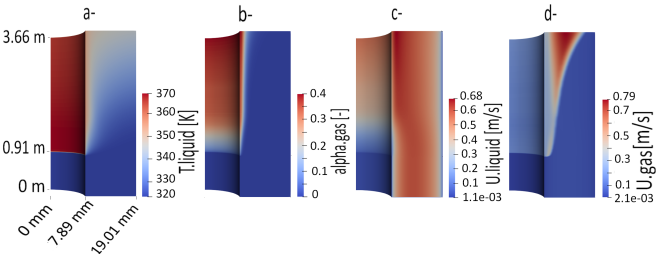

Figure 2. CFD fields spatial distributions: a- Liquid temperature, b- Void fraction, c- Liquid velocity and d- Vapor velocity.

The working fluid R-113 enters the concentric pipe at a uniform velocity distribution, with a mean equal to 0.522 m/s, and an inlet temperature equal to 50.2°C, representing 30.3°C below the saturation temperature. Along the adiabatic section, from the inlet downward to 0.91 m, where heating starts, the void fraction showed through Figure 2(b) maintains a zero value, meaning that there is no bubble formation and no phase change, corresponding to a constant liquid temperature equal to the inlet temperature, as presented by Figure 2(a). As can be deduced from Figure 2(c), the liquid velocity in the adiabatic flow section follows a parabolic profile, where it is zero in the viscous boundary layer at the wall, where the non-slip boundary condition is applied. In this section, the flow is being developed, with an average Reynolds number at 34450, referring to a turbulent flow. In the heated flow section, the void fraction starts having values higher than zero, corresponding to bubbles nucleation at the heated surface. Nucleation starts when the local liquid temperature in the heated surface vicinity reaches the saturation temperature, corresponding to the local system pressure. The void fraction at the heated surface increases with increasing heated length, up to a maximum value of 40% near the outlet. However, it decreases with increasing radial distance from the heated surface, to become zero far away from it. This is the typical subcooled nucleate boiling heat transfer regime, where the bubbles are formed at the heated surface, giving the highest radial void fraction. This latter will decrease when increasing the radial distance from the heated surface, due to the absence of evaporation far from the wall, and bubbles are subject to condensation, since the liquid is still subcooled and the surrounding bubbles temperature gradually drops below the saturation. This also can be proved by the liquid temperature distribution presented in Figure 2(a). When entering the heated flow section at a temperature equal to the inlet temperature, the liquid near the heated surface starts to heat up until it reaches its saturation temperature, at which evaporation at the wall occurs. Far from the heated surface in the radial direction, the liquid is heated, but it does not reach its saturation temperature and is still subcooled. The bubbles which left their nucleation sites will condense in this flow region. A special behavior of the liquid phase velocity at the viscous boundary layer near the heated surface is observed. The liquid velocity reaches its maximum

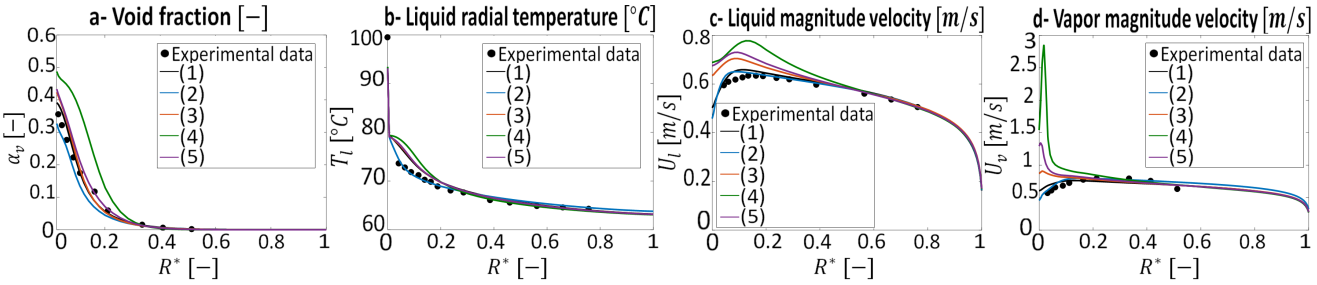

Figure 3. Interfacial forces effect on the radial boiling fields. Experimental data of Roy et al. (2001). a- Void fraction prediction, b- Liquid radial temperature, c- Liquid magnitude velocity and d- Vapor magnitude velocity. Legend: (1) Schiller and Naumann (1935) drag force model, Antal et al. (1991) wall lubrication force model and Burns et al. (2004) turbulent dispersion force model with $C_{TD} = 1$. (2) Tomiyama et al. (1998) drag model, Frank (2005) wall lubrication force model and Burns et al. (2004) turbulent dispersion force model with $C_{TD} = 1$. (3) Schiller and Naumann (1935) drag force model, neglected wall lubrication force and Burns et al. (2004) turbulent dispersion force model with $C_{TD} = 1$. (4) Schiller and Naumann (1935) drag force model, neglected wall lubrication force and Lopez de Bertodano (1991) turbulent dispersion model with $C_{TD} = 0.4$. (5) Schiller and Naumann (1935) drag force model, neglected wall lubrication force and Lopez de Bertodano (1991) turbulent dispersion force model with $C_{TD} = 1$.

near the wall, under the effect of the bubble nucleation and motion. This is a feature of boiling flows, where the liquid velocity which approaches zero near the adiabatic walls becomes increasingly higher at the heated section of the wall, away from the non-slip boundary condition. This yields increased heat transfer coefficients hence enhancing the heat transfer from the heated wall to the bulk liquid. At the external adiabatic wall, in both flow regions, adiabatic and heated, the liquid velocity keeps the parabolic profile, where it is very low in the viscous boundary layer. Concerning the vapor phase velocity, Figure 2(c) shows that the vapor velocity increases with increasing void fraction and the two-phase layer thickness.

The CFD predictions of the radial profiles of the quantities of concern, i.e., void fraction, liquid temperature, liquid and vapor velocities, following the measurement section used by Roy et al. (2001), located at 2.894 m downward the concentric pipe inlet are presented through Figure 3. The dimensionless distance R^* is calculated as $(r - r_{in})/r_{out}$. These predicted fields are compared against the available experimental data of Roy et al. (2001). In order to quantify the interfacial forces effect on the CFD simulation results, different interfacial forces were taken into account or neglected, employing the most relevant force models for boiling. In Figure 3, the studied forces are the drag force, the wall lubrication force and the turbulent dispersion force. The drag force is taken into account in all the simulations, where the models of Schiller and Naumann (1935) and Tomiyama et al. (1998) are compared, while the turbulent dispersion force is modeled based on Burns et al. (2004) and Lopez de Bertodano (1991). However, the wall lubrication force is taken into account in some simulations only and neglected in others, in order to quantify its effect on boiling. The models of Antal et al. (1991) and Frank (2005) are tested. The results presented by Figure 3 are obtained for a constant added mass coefficient model set to 0.5, and a neglected lift force. As it can be seen in Figure 3(a), a successful prediction of the void fraction with comparison to the experimental data is obtained with the drag model of Schiller and Naumann (1935), the wall lubrication force of Antal et al. (1991) and the turbulent dispersion force of Burns et al. (2004), with a turbulent dispersion coefficient $C_{TD} = 1.0$. These interfacial forces models give also fair predictions of the liquid and vapor phase velocities, presented by Figures 3(c) and 3(d), respectively. However, using these models will yield to an over-estimation of the liquid temperature in the two-phase boundary layer near the heated surface, as it can be seen in Figure 3(b). The successful predictions of the liquid and vapor phase velocities and the liquid phase temperature are obtained by the predictions associated to the drag model of Tomiyama et al. (1998), the wall lubrication model of Frank (2005) and the turbulent dispersion model of Burn et al. (2004), with $C_{TD} = 1.0$. Nevertheless, these models yield to a small underestimation of the void fraction in the vicinity of the heated surface. Then, neglecting the wall lubrication force will affect considerably the predictions accuracy. Based on the comparison against the available experimental data, the predictions associated with neglecting the wall lubrication force overestimate all the considered fields. The turbulent dispersion model of Lopez de Bertodano (1991) gives always high over-prediction, and the highest one is associated with a lower turbulent dispersion force coefficient of C_{TD}. This drag model with a lower C_{TD} is giving also the highest over-prediction of the liquid radial temperature and velocity. However, a failed prediction of the vapor phase velocity is obtained when the Lopez de Bertodano (1991) turbulent dispersion model is employed, regardless of the value of C_{TD}, especially in the two-phase boundary layer near the heated surface. Despite the overestimations of the Burns et al. (2004) turbulent dispersion model when neglecting the wall lubrication force, the predictions are fair for the void fraction and the liquid radial temperature. Nonetheless, for the liquid and the vapor phase velocities, the predictions associated with the latter mentioned models are failed, especially at the heated surface, where overly high velocities are obtained. The

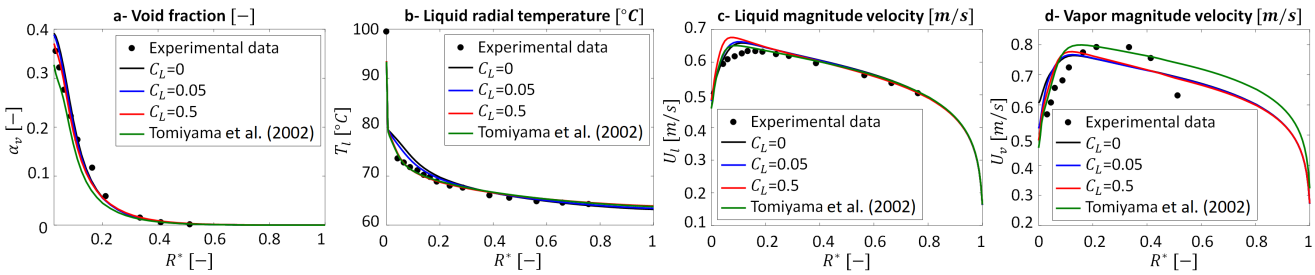

Figure 4. Lift force effect on the radial boiling fields. Experimental data of Roy et al. (2001) a- Void fraction prediction, b- Liquid temperature, c- Liquid velocity, d- Vapor velocity.

two-phase boundary layer thickness, where bubbles are present and subject to nucleation and condensation, is very well predicted using any interfacial force model, as it can be deduced from the estimated void fraction comparison with the experimental data through Figure 3(a). Hence, when neglecting the lift force, whose effect on boiling will be discussed in the next paragraph, and setting a constant added mass coefficient equal to 0.5 as well as neglecting the wall lubrication force will yield an over-estimation of all the considered fields, and this overestimation is amplified when a low turbulent dispersion model is used. The models yielding the best void fraction prediction will over-predict the other fields considered, and the successful predictions of the liquid radial temperature, liquid and vapor velocities will give a small under-prediction of the void fraction.

The lift force effect on the CFD predicted fields is quantified in Figure 4. Two different lift models are compared here, a constant lift coefficient model, set to 0.05 and 0.5, and the lift coefficient model of Tomiyama et al. (2002). When a constant lift coefficient model is employed, then the Schiller and Naumann (1935) drag force model, the Antal et al. (1991) wall lubrication force model and the Burns et al. (2004) turbulent dispersion force model are used. For the Tomiyama et al. (2002) lift model, Tomiyama et al. (1998) drag model, the Frank (2005) wall lubrication force model and Burns et al. (2004) turbulent dispersion force are employed. In all the performed simulations of Figure 4, the added mass force was taken into account via a constant value set to 0.5. The comparison with the experimental data shows that deviations between the tested models are minor. The Tomiyama et al. (2002) lift model gives the best predictions for the liquid radial temperature, liquid velocity and vapor velocity, with comparison to the experimental data, presented respectively through Figures 4(b), 4(c) and 4(d). However, a small underestimation is observed for the void fraction illustrated in Figure 4(a). This trend is observed in the results of Figure 3(a) when the Tomiyama et al. (1998) drag model, the Frank (2005) wall lubrication model and the Burns et al. (2004) turbulent dispersion model are used. The authors believe that this underestimation is caused by the interfacial models, except with the Tomiyama et al. (2002) lift model, and that its effect on the CFD calculations is minor. Despite the small differences obtained when different constant lift coefficients C_L are used, the best prediction is obtained when $C_L = 0.5$ for void fraction. However, the corresponding liquid velocity is very high near the heated surface, and this will yield to over-predictions of the heat transfer. Comparable results are observed when performing the calculations with $C_L = 0.05$ and neglecting the lift ($C_L = 0$). Hence, despite its importance in two-phase bubbly flows, the lift force has a minor effect when phase change is considered. Hence, this force can be neglected when modeling boiling flows.

5 Conclusions

In this work, 2D axisymmetric CFD simulations were carried out to model the subcooled nucleate boiling flow of refrigerant R-113 flowing upward a narrow concentric pipe. The void fraction spacial distribution showed that boiling starts at the heated section, and the highest values are obtained near the heated surface where nucleation occurs, corresponding to the local saturation temperature. The temperature field showed that the saturation temperature is reached near the heated surface, and that the liquid stills subcooled away from the heated surface, which allows the bubbles to leave the heated surface and condense. This will yield to decreased values of the void fraction, to reach zero at the end of the two-phase layer. The velocity field proved that higher values are obtained at the heated surface, under the effect of the bubbles nucleation and motion, and this is one of the most important boiling flows features, leading to an increased values of the heat transfer coefficient, that was very well predicted by the current CFD simulations.

A sensitivity analysis of the acting interfacial forces models was performed by comparing the obtained CFD predictions with the experimental data of Roy et al. (2001). It was shown that all the interfacial forces, except the lift, have a considerable effect on the predicted fields. Neglecting the wall lubrication force will yield to increased values of the void fraction, liquid radial temperature near the heated surface and liquid phase velocity. This will lead to failed predictions of the vapor phase velocity. It was shown also that the models giving the best void fraction predictions will give small overestimations of the other fields, and models giving successful predic-

tions of the liquid radial temperature and the velocities of the liquid and vapor phases will slightly under-predict the corresponding void fraction. It was proven that the lift force has a minor effect on the predicted fields, and it can be neglected in CFD simulations of subcooled boiling flows without any major concern.

The present work provides a knowledge foundation for performing CFD simulations of subcooled nucleate boiling flows of refrigerants. It provides guidance on the corresponding interfacial forces that should be taken into account, with model recommendations provided for better accuracy with respect to each important boiling regions. Future improvement of this work can be recapitalized in using IATE model to predict the bubbles bulk diameter instead of a constant model, as adopted in this work. Also, the interfacial forces analysis should be complemented by turbulence model quantification.

Acknowledgments

The authors gratefully acknowledge ABB AB, Westinghouse Electric Sweden AB, HITACHI ABB Power Grids and the Swedish Knowledge Foundation (KKS) for their support and would like to particularly thank ABB AB for providing the HPC platform.

References

H. Anglart and O. Nylund. CFD application to prediction of void distribution in two-phase bubbly flows in rod bundles. *Nuclear Engineering and Design*, 163(1):81 – 98, 1996. doi:10.1016/0029-5493(95)01160-9.

S. P. Antal, R. T. Lahey Jr, and J. E. Flaherty. Analysis of phase distribution in fully developed laminar bubbly two-phase flow. *International Journal of Multiphase Flow*, 17 (5):635 – 652, 1991. doi:10.1016/0301-9322(91)90029-3.

A. D. Burns, T. Frank, I. Hamill, and J. M. Shi. The Favre averaged drag model for turbulent dispersion in Eulerian multiphase flows. In *Proceedings - 5th International Conference on Multiphase Flow, ICMF'04*, Yokohama, Japan, May 2004.

R. Cole. A photographic study of pool boiling in the region of the critical heat flux. *AIChE Journal*, 6(4):533 – 538, 1960. doi:10.1002/aic.690060405.

Y. Egorov and F. Menter. Experimental implementation of the RPI wall boiling model in CFX-5.6. Technical report, ANSYS/TR-04-10, 2004.

T. Frank. Advances in computational fluid dynamics (CFD) of 3-dimensional gas-liquid multiphase flows. In *Proceedings - NAFEMS Seminar: "Simulation of Complex Flows (CFD)"*, Niedernhausen/Wiesbaden, Germany, April 2005.

M. Ishii, S. Kim, and J. Kelly. Development of interfacial area transport equation. *Nuclear Engineering and Technology*, 37 (6):525–536, 2005.

B. Končar and E. Krepper. CFD simulation of convective flow boiling of refrigerant in a vertical annulus. *Nuclear Engineering and Design*, 238(3):693 – 706, 2008. doi:10.1016/j.nucengdes.2007.02.035.

B. Končar, I. Kljenak, and B. Mavko. Modelling of local two-phase flow parameters in upward subcooled flow boiling at low pressure. *International Journal of Heat and Mass Transfer*, 47(6):1499 – 1513, 2004. doi:10.1016/j.ijheatmasstransfer.2003.09.021.

N. Kurul and M. Z.. Podowski. Multidimensional effects in forced convection subcooled boiling. In *Proceedings - International Heat Transfer Conference Digital Library*. Begel House Inc., 1990.

J.C. Lai and B. Farouk. Numerical simulation of subcooled boiling and heat transfer in vertical ducts. *International Journal of Heat and Mass Transfer*, 36(6):1541 – 1551, 1993. doi:10.1016/S0017-9310(05)80064-X.

M. Lemmert and J. M. Chawla. Influence of flow velocity on surface boiling heat transfer coefficient. *Heat Transfer in Boiling*, pages 237–247, 1977.

M. Lopez de Bertodano. *Turbulent bubbly flow in a triangular duct*. PhD thesis, Rensselaer Polytechnic Institute, New York, USA, 1991.

E. Michta. Modeling of subcooled nucleate boiling with OpenFOAM. Master's thesis, KTH Royal Institute of Technology, Stockholm, Sweden, 2011.

A. Rabhi and R. Bel Fdhila. Evaluation and analysis of active nucleation site density models in boiling. In *Proceedings - The Second Pacific Rim Thermal Engineering Conference*, Maui, Hawaii, USA, December 2019.

W. E. Ranz and W. R. Marshall. Evaporation from drops. *Chemical Engineering Progress*, 48(3):141–146, 1952.

R. P. Roy, S. Kang, J. A. Zarate, and A. Laporta. Turbulent Subcooled Boiling Flow—Experiments and Simulations . *Journal of Heat Transfer*, 124(1):73–93, 2001. doi:10.1115/1.1418698.

Y. Sato, M. Sadatomi, and K. Sekoguchi. Momentum and heat transfer in two-phase bubble flow—II. A comparison between experimental data and theoretical calculations. *International Journal of Multiphase Flow*, 7(2):179 – 190, 1981. doi:10.1016/0301-9322(81)90004-5.

L. Schiller and Z. Naumann. A drag coefficient correlation. *Zeit. Ver. Deutsch. Ing.*, 77:318–320, 1935.

V. I. Tolubinsky and D. M. Kostanchuk. Vapour bubbles growth rate and heat transfer intensity at subcooled water boiling. In *Proceedings - International Heat Transfer Conference 4*, volume 23. Begel House Inc., 1970.

A. Tomiyama, I. Kataoka, I. Zun, and T. Sakaguchi. Drag coefficients of single bubbles under normal and micro gravity conditions. *JSME International Journal*, 41(2):472–479, 1998.

A. Tomiyama, G. P. Celata, S. Hosokawa, and S. Yoshida. Terminal velocity of single bubbles in surface tension force dominant regime. *International Journal of Multiphase Flow*, 28 (9):1497 – 1519, 2002. doi:10.1016/S0301-9322(02)00032-0.

N. Zuber. On the dispersed two-phase flow in the laminar flow regime. *Chemical Engineering Science*, 19(11):897 – 917, 1964. doi:10.1016/0009-2509(64)85067-3.